Carbohydrate Research 388 (2014) 50–60

Contents lists available at ScienceDirect

Carbohydrate Research

journal homepage: www.elsevier.com/locate/carres

Free energy landscape for glucose condensation and dehydration reactions in dimethyl sulfoxide and the effects of solvent

Xianghong Qian [a,*], Dajiang Liu [b]

[a] Department of Chemical Engineering, University of Arkansas, Fayetteville, AR 72701, United States
[b] Department of Mechanical Engineering, Colorado State University, Ft Collins, CO 80521, United States

ARTICLE INFO

Article history:
Received 15 November 2013
Received in revised form 30 January 2014
Accepted 7 February 2014
Available online 18 February 2014

Keywords:
Glucose
DMSO
Free energy surface
Condensation
Dehydration

ABSTRACT

The mechanisms and free energy surfaces (FES) for the initial critical steps during proton-catalyzed glucose condensation and dehydration reactions were elucidated in dimethyl sulfoxide (DMSO) using Car–Parrinello molecular dynamics (CPMD) coupled with metadynamics (MTD) simulations. Glucose condensation reaction is initiated by protonation of C1—OH whereas dehydration reaction is initiated by protonation of C2—OH. The mechanisms in DMSO are similar to those in aqueous solution. The DMSO molecules closest to the C1—OH or C2—OH on glucose are directly involved in the reactions and act as proton acceptors during the process. However, the energy barriers are strongly solvent dependent. Moreover, polarization from the long-range electrostatic interaction affects the mechanisms and energetics of glucose reactions. Experimental measurements conducted in various DMSO/Water mixtures also show that energy barriers are solvent dependent in agreement with our theoretical results.

1. Introduction

Glucose is the most important and abundant monomeric sugar on earth. Elucidating glucose transformations and reactions is critical to our understanding and manipulation of this vital molecule. Our earlier theoretical studies[1–9] and experimental results[1,10–13] show that proton catalyzed glucose reactions are generally not selective due to multiple protonation sites on the glucose molecule leading to multiple reaction pathways. Protonation of the O5 on the glucose ring leads to the mutarotation between α- and β-glucose. Protonation of the C1—OH on glucose leads to the formation of an oxocarbenium carbocation and the eventual 1, *x* (*x* = 2, 3, 4, 6) linked oligosaccharides from condensation reactions. Protonation of C2—OH on glucose leads to the formation of 5-hydroxylmethylfurfural (HMF) from dehydration reaction as well as isomerization reaction to fructose. In addition, our earlier results[1–9] indicate that protonation of the ring O or the hydroxyl groups on the glucose molecule and the subsequent breakage of the C—O bond is the rate-limiting step. Moreover, it was found that glucose reactions are strongly solvent dependent due to the competition for proton from the solvent molecules. The reaction barriers are largely solvent induced. Our earlier studies focused on the glucose mutarotation,[14] condensation,[6] isomerization[9] and dehydration[7] reactions in aqueous solutions. Here the critical initial steps during glucose condensation and dehydration reactions in dimethyl sulfoxide (DMSO) are investigated.

Car-Parrinello[15] based ab initio molecular dynamics (CPMD)[16] coupled with metadynamics (MTD)[17] simulations have been successful in elucidating the mechanisms, the rate-limiting steps, and associated barriers as well as free energy surfaces (FES) for glucose reactions in aqueous solutions.[6,7,9,14] For example, excellent agreement was obtained between the calculated and experimental barriers for glucose mutarotation,[14] condensation,[5,6] isomerization[9], and dehydration[7] reactions. Here CPMD–MTD simulations for glucose condensation and dehydration reactions in DMSO solvent medium are conducted to gain insights into the effects of solvent on the mechanisms and barriers for glucose reactions. Moreover, atomic charges of the glucose molecule in the gas phase as well as in H_2O and DMSO solvents were calculated using both Gaussian09[18] and CPMD in order to gain deep insight into the solvent effects on glucose reactivity.

In order to validate our theoretical results, experiments were also conducted for glucose reactions in pure DMSO and several DMSO/Water mixtures at temperatures ranging from 120 °C (393 K) to 140 °C (413 K). The concentrations of glucose, major reaction products, and their time dependence were determined using Nuclear Magnetic Resonance (NMR). Moreover, activation energy barriers in the solvent mixtures for glucose degradation, its dehydration to 1,6-anhydro-β-D-glucopyranose (levoglucosan) and HMF were determined and compared with theoretical results.

* Corresponding author. Tel.: +1 479 575 8401.
E-mail address: xqian@uark.edu (X. Qian).

http://dx.doi.org/10.1016/j.carres.2014.02.010
0008-6215/

2. Computational details

CPMD–MTD allows for efficient and accelerated sampling of chemical and biological processes for free energy calculations, particularly for chemical reactions involving the bond-breaking and bond-forming processes in the time scale not accessible by the conventional methods. The acceleration of the sampling process is achieved by filling the reactant and product wells with repulsive bias potentials[17,19] to facilitate barrier crossing. Once the reactant well is filled with potentials close enough to the reaction barrier, the system overcomes the barrier and moves to the product well. When the product well is also filled and the FES becomes flat, the system is able to sample the reactant and product states randomly without any barrier. The original FES of the system is subsequently reconstructed based on the amount of bias potentials added to reach the flat FES state. This method assumes that several collective variables (CV), which distinguish the initial state from the final state, are able to characterize the slow, rate-limiting steps.

The left panel in Figure 1 shows the CVs for the critical steps during glucose condensation (left panel) and dehydration (right panel) reactions. Our previous results[6] for glucose condensation reaction in aqueous solution show that the rate-limiting step involves the protonation of C1—OH and the breakage of the C1—O1 bond. The C1 carbocation formed and subsequently the more stable oxocarbenium ion are the critical intermediates for various 1, x (x = 2,3,4,6) linked disaccharides. For glucose condensation reaction in DMSO, a similar mechanism is assumed. As a result, CVs for the first steps in glucose condensation reaction comprise protonation of C1—OH (CV2) and breakage of C1—O1 bond (CV1). In addition, our earlier studies[5,6] in aqueous solution also show that partial dehydration due to the migration of the hydronium ion to the neighborhood of the sugar molecule also contribute substantially to the barrier for condensation reaction.

Three CVs are needed for the critical steps during glucose dehydration to form a cyclic HMF intermediate in aqueous solution as shown in the right panel of Figure 1. Glucose dehydration reaction is initiated by the protonation of C2—OH, the breakage of the C2—O2 bond, and the formation of C2—O5 bond leading to the formation of a five-member aldehyde ring intermediate.[7] However, our previous results[7] show that proton partial dehydration does not contribute to the barrier for glucose dehydration reaction in aqueous solution since the barrier of 30–35 kcal/mol is dominated by protonation followed by the breakage of the C2—O2 bond only. Once a C2-carbocation is formed, the formation of C2—O5 bond appears to be spontaneous without any barrier. In this study, an analogous mechanism for glucose dehydration to HMF in DMSO was investigated. However, it does not exclude the possible existence of an alternative reaction pathway in DMSO. Similar to aqueous solution, three CVs are adopted for proton-catalyzed glucose dehydration to HMF in DMSO. These three CVs comprise protonation of C2—OH (CV3), the breakage of the C2—O2 bond (CV1), and the formation of C2—O5 bond (CV2).

Our earlier studies[5–9,20] showed that CVs using coordination numbers (CN) are effective for exploring sugar reaction processes. The equation of CN[19] is given by

$$CN(i,j) = \frac{1 - \left(\frac{d_{ij}}{d_0}\right)^p}{1 - \left(\frac{d_{ij}}{d_0}\right)^q},$$

where d_{ij} is the distance between atoms i and j, d_0 is the cutoff distance, and p and q are high-power integers used to distinguish between the coordinated and non-coordinated states. The values $p = 6$ and $q = 12$ are typically chosen for calculating the CNs. The choice for the cutoff distance d_0 depends on the specific bond. For C–O and O–H bonds, values of 2.0 and 1.5 Å are usually chosen for d_0 respectively as is done here and previously in our work.[5–7,9]

The dynamics of the CVs are controlled by the force constant k and fictitious mass m. The values of $k = 2.0$ au and $m = 100$ amu were used for all the CVs here. The bias potential chosen is a commonly used Gaussian functional. The height and the width of the Gaussian bias potential were chosen to be 0.001 and 0.100 au respectively for all the simulations. The bias potentials were added whenever the displacements in the CVs were larger than 1.5 times the width, but no shorter than 100 MD steps. Studies have shown that this choice of parameters is efficient with uncertainty in the range of 1–2 kcal/mol.[21] More details on the method applied to sugar reactions could be found in our earlier work.[5–9,20]

The simulations were conducted using the Becke,[22] Lee, Yang, and Parr (BLYP)[23] functional for the valence and semi-core electrons. Goedecker[24] pseudopotential was used for the core electrons. The energy cut-off of 80 Ry was used for the plane wave basis set. The combinations of these parameters have found to yield excellent structural properties as well as energetics and reactivity for sugar molecules.[25,26] The simulations were conducted under constant volume and constant temperature (NVT) with a Nosé–Hoover chain thermostat.[27,28] The temperature was kept at 27 °C (300 K) for the condensation reaction initiated by the protonation of C1—OH and at 227 °C (500 K)for the dehydration reaction initiated by the protonation of C2—OH. To effectively separate the fast motions of the electrons from the slow movement of the nuclei, a

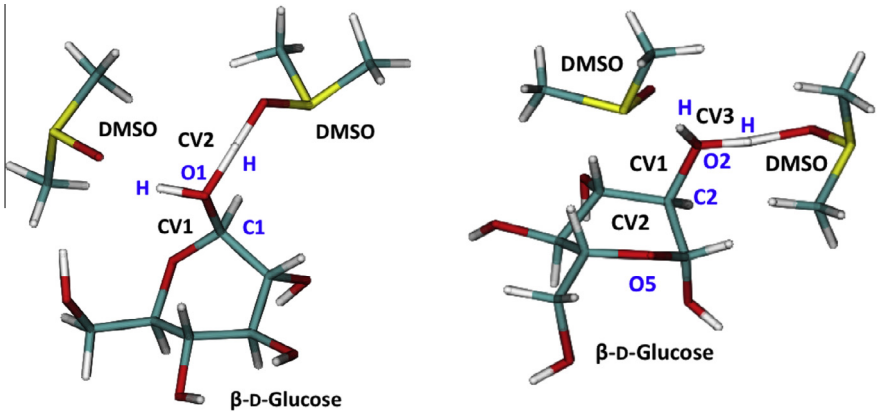

Figure 1. The collective variables (CVs) for critical steps during glucose condensation reaction are shown in the left panel with CV1 representing C1—O1 bond and CV2 representing O1—H bond. CVs for critical steps during glucose dehydration reaction are shown in the right panel with CV1 representing C2—O2 bond, CV2 representing C2—O5 bond and CV3 representing O2—H bond.

fictitious mass of 800 amu and a time step of 0.125 femtosecond (fs) were used. The system contains one glucose molecule, 40 DMSO molecules, one proton, and one Cl^- counter ion. The initial unit cell containing only one glucose and 40 DMSO molecules was equilibrated for over 10 picoseconds (ps) using CPMD. After the initial equilibration, one H^+ and one Cl^- ion were then inserted in the system to mimic the acidic environment. The unit cell has a dimension of $18.5 \times 18.5 \times 18.5$ Å^3 with a density of 0.88 g/cm^3. Periodic boundary conditions (PBC) were applied. Ewald summation[29] was used to integrate the long-range electrostatic interaction energies.

The atomic charges derived from the electrostatic potentials (ESP)[30] based on a method developed by Hirshfeld[31] were determined using CPMD for the glucose molecule in the gas phase as well as solvated by explicit DMSO or H_2O molecules. Atomic charges were determined both with and without periodic boundary conditions. A plane-wave cut-off of 100 Ry with BLYP functional was used. For comparison, ESP charges were also calculated using Gaussian09 for the glucose molecule in the gas phase as well as when solvated implicitly by DMSO or H_2O. The hybrid B3LYP potential with 6-311++G** basis set coupled with implicit CPCM solvation model[32,33] were used for the ESP charge calculations using Gaussian09.

3. Experimental procedures

3.1. Materials and methods

NMR spectra were recorded either by Varian Inova 300 (FT 300 MHz) or Varian Inova 400 spectrometer. Chemical shifts for ^{1}H spectra are reported as parts per million (ppm) relative to tetramethylsilane (TMS). Concentrations were determined based on the ratios of peak areas for the products to those of biphenyl (internal reference). Typical NMR spectra of glucose, 1,6-anhydro-D-β-glucopyranose (levoglucosan, AHG), fructose, and HMF were listed in the Supporting information (SI).

D-Glucose (Fisher Chemical), D-fructose (Mallinckrodt), biphenyl (Aldrich), 5-hydromethylfurfural (HMF) (Aldrich) were purchased and used without further purification. DMSO-d_6 and D_2O were used for all the NMR experiments. Reactions were conducted in the oil-bathed NMR tubes. Reaction solutions were prepared beforehand to ensure their homogeneity. Different ratios of DMSO/D_2O solvent mixtures with pure DMSO, DMSO/D_2O = 95/5 (v/v), DMSO/D_2O = 90/10 (v/v), DMSO/D_2O = 80/20 (v/v) were used for the reactions. Small amount of hydrochloric acid (HCl) was added as a catalyst. Biphenyl was used as an internal reference.

3.2. Representative procedure for glucose conversion in DMSO/Water

Glucose reactions and subsequent NMR experiments were conducted in a closed lid NMR tube due to the volatility of HCl acid catalyst. Solutions of glucose (56 mM) in various ratios of DMSO/Water mixtures with HCl (5.6 mM) and biphenyl (2 mM) were prepared in advance. Each NMR tube evenly charged with 0.6 mL solution was then placed into the pre-equilibrated oil-bath at pre-determined temperatures. Reactions were quenched by rapidly inserting the tubes into ice water. Subsequent NMR ^{1}H experiments were performed. The ^{1}H NMR peaks used for quantification: biphenyl δ 7.66 (m, 1H, H3), 7.46 (m, 1H, H2), 7.36 (m, 1H, H1); glucose δ 4.94 (d, 1H, J = 3.6 Hz, H1-α), 4.20 (d, 1H, J = 7.5 Hz, H1-β); for levoglucosan δ 5.15 (s, 2H, H1-β), 4.76 (dd, 1H, H3); for HMF, δ 9.54 (s, 1H, H1), 7.49 (d, 1H, J = 3.6 Hz, H2), 6.60 (d, 1H, J = 3.6 Hz, H3), 4.50 (s, 2H, H6).

4. Results and discussion

4.1. The mechanism and free energy surface for glucose condensation reaction in DMSO

Figure 2 shows the mechanism for the critical steps during glucose condensation reaction involving protonation of C1—OH and the formation of an oxocarbenium ion from the CPMD–MTD simulations. Only two DMSO molecules involved directly in the reaction are shown in Figure 2. A total of over 800 MTD simulation steps were conducted for the reaction. The initial state (***A***) includes a proton attached to the S═O group on the closest DMSO molecule. During the subsequent simulations, this proton and the other proton initially bonded to O1 transfer back and forth between the S═O groups on the two neighboring DMSO molecules and C1—OH on the glucose ring as shown in Figure 2 (B and C). Since the two protons are identical, both of the two closest DMSO molecules are directly involved in the proton transfer process. Finally, the protonated OH group (i.e. H_2O) departs from the glucose ring leading to the formation of C1-carbocation and the more stable oxocarbenium ion (***D***).

Even though the mechanism for glucose condensation reaction in DMSO is similar to the corresponding reaction in the aqueous solution, the role of solvent appears to be rather different. In the simulations conducted in aqueous solution, the water molecules form extensive hydrogen bonding network. The excess proton can transport rapidly within the water cluster without any barrier via this extensive hydrogen-bonding network. The high mobility of the proton in the water cluster indicates its stability in aqueous solution due to the significant contribution from entropy. Further the small positively charged hydronium ion has a very large hydration free energy of about −264 kcal/mol[34,35] further suggesting the stability of proton in water. As a result, a barrier of about 25 kcal kcal/mol from both experiments[13] and theoretical calculations[6,36] was estimated for glucose condensation reaction in aqueous solution. The contribution to this barrier comes from partial proton dehydration due to its migration from the bulk solvent to the neighborhood of the glucose molecule as well as the protonation of the C1—OH and the formation of the stable intermediate oxocarbenium ion. For glucose condensation reaction in DMSO, a proton can only attach to its closest DMSO molecule thus only two nearest neighboring DMSO molecules are involved directly in the reaction process. Proton solvation free energy in DMSO is estimated to be −273.3 kcal/mol,[36] slightly larger than the corresponding value in water. Since the proton affinity and proton solvation free energy in DMSO are different from those in water, the reaction barrier for protonation of C1—OH in DMSO is expected to be different as is confirmed from our CPMD–MTD results discussed in more detail below.

Figure 3 shows the fluctuations of the two CVs during the course of almost 900 CPMD–MTD simulation steps. The blue line representing CV1 (C1—O1) describes the bond breakage and formation between C1 and O1 whereas the red line representing CV2 (O1—H) describes the protonation of C1—OH process. It can be seen that proton initially bonded to the O on DMSO was rapidly transferred to the C1—OH in less than 20 MTD steps. However, the C1—O1 bond did not break to form a C1-carbocation until about about 50 MTD steps. The sampling of the C1-carbocation is rather brief as the proton was seen to transfer back to the neighboring DMSO molecules and the neutral glucose molecule reforms. The C1—O1 bond is again broken at around 300 MTD steps after the proton transfers again to the C1—OH. The protonated hydroxyl group (i.e. H_2O) departs from the glucose ring to form an oxocarbenium ion.The oxocarbenium cation was sampled during the subsequent 225 MTD steps. At around 490 MTD steps, the proton again

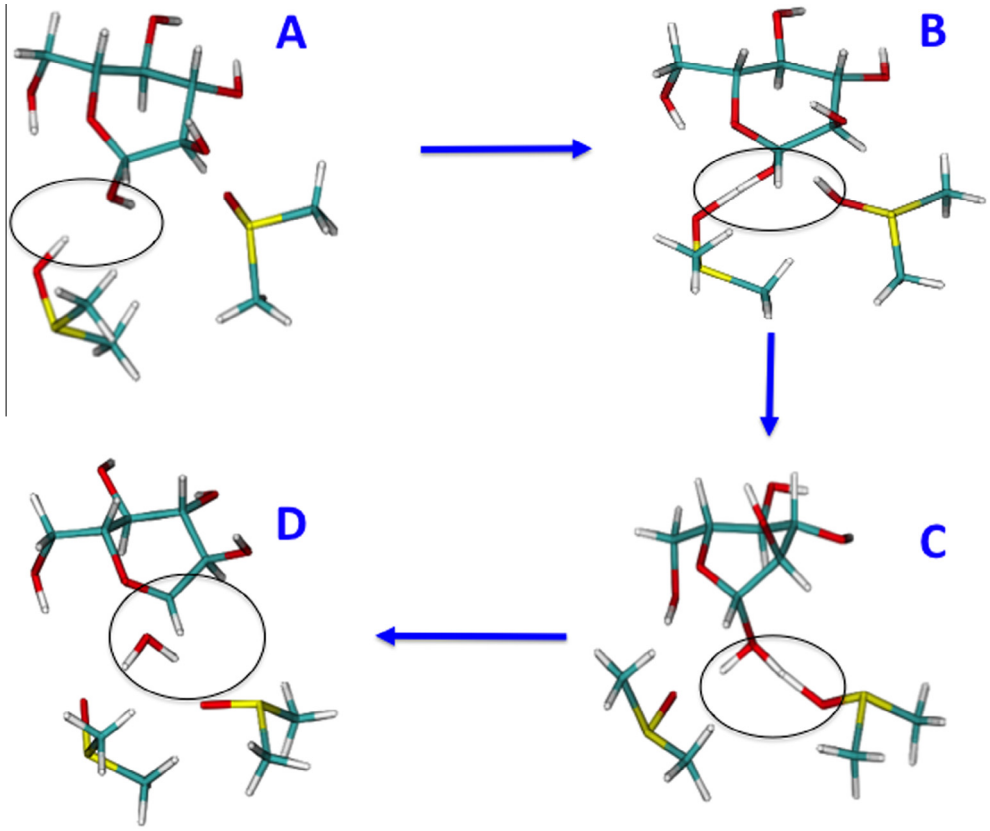

Figure 2. The mechanism for protonation of C1—OH on glucose and the subsequent formation of oxocarbenium ion during glucose condensation reaction in DMSO (O (red), C (cyan), S (yellow), and H (white)). Only two participating DMSO molecules are shown. The reactive sites are circled. (For interpretation of the references to color in this figure legend, the reader is referred to the web version of this article.)

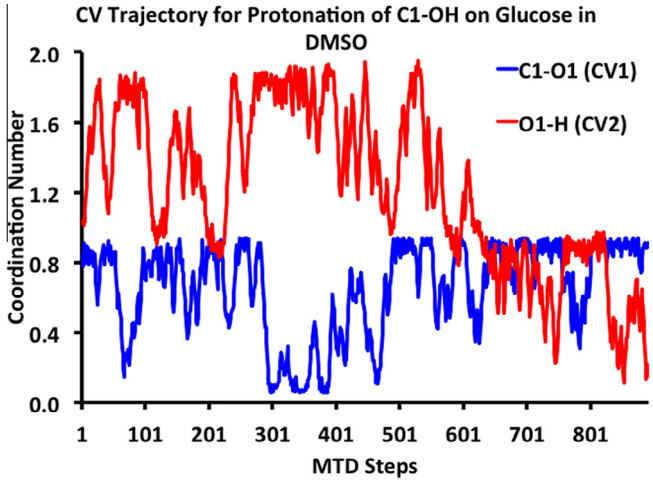

Figure 3. The variation of the CV1 (C1—O1, blue) and CV2 (O1—H, red) during the CPMD–MTD simulations for glucose condensation reaction in DMSO initiated by protonation of C1—OH. (For interpretation of the references to color in this figure legend, the reader is referred to the web version of this article.)

transfers back to the neighboring DMSO molecule and the C1—O1 bond reforms. Subsequently the proton was seen transferring back and forth between the C1—OH and the S=O on the neighboring DMSO molecules. At 825 MTD steps, both protons transfer to the neighboring DMSO molecules forming a different chemical species. This completes the sampling process for the protonation of C1—OH and the formation of the oxocarbenium ion. The FES was reconstucted based on the 825 MTD simulations.

Based on the amount of Gaussians potentials filled, the FES was reconstructed. Figure 4 shows the projected two dimensional (2D) free energy contour plot between CV1 (C1—O1) and CV2 (O1—H). The general feature of FES for protonation of C1—OH on glucose and the breakage of C1—O1 bond in DMSO is similar to the reaction carried out in water. The stable or metastable structures during the reaction process include the initial neutral glucose molecule when

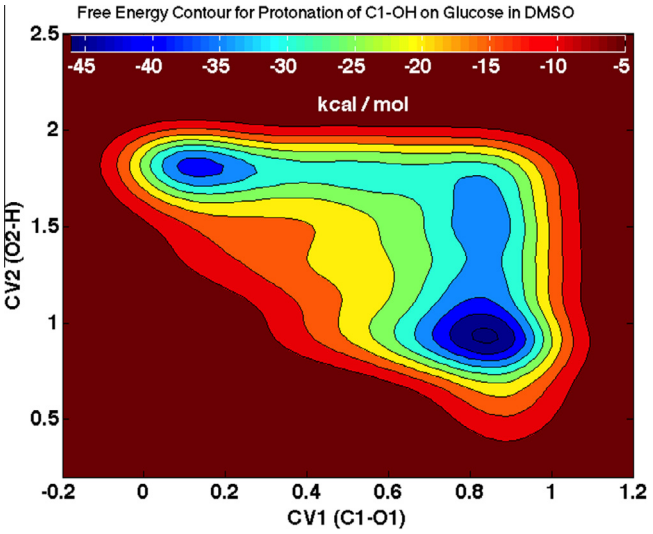

Figure 4. The projected free energy contour plot between CV1 (C1—O1) and CV2 (O1—H) for protonation of C1—OH and breakage of C1—O1 bond during glucose condensation reaction in DMSO.

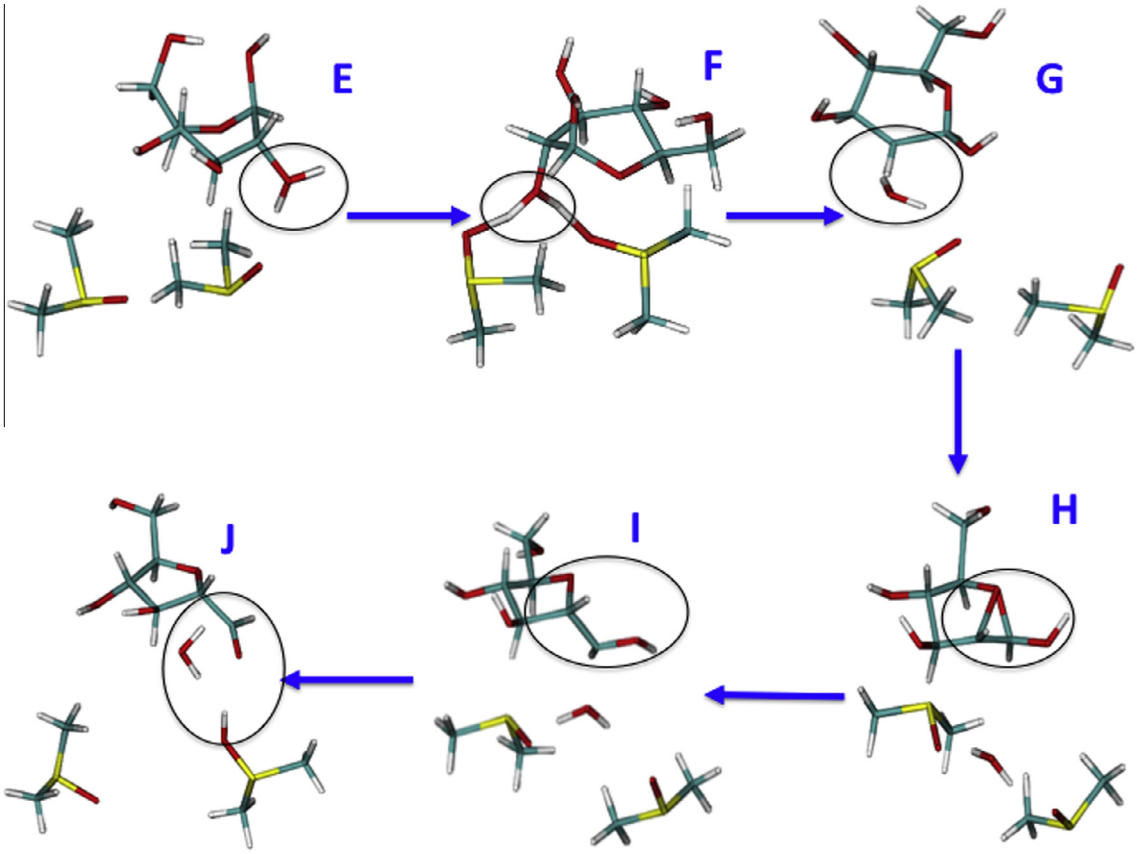

Figure 5. The mechanism for glucose dehydration reaction to form a HMF intermediate via a direct cyclic pathway initiated by protonation of C2—OH, breakage of the C2—O2 bond, and the formation of the C2—O5 bond. Only the DMSO molecules directly participating in the reaction are shown. The reactive sites are shown in circles.

the proton is attached to the neighboring DMSO molecule, the final oxocarbenium ion after the breakage of the C1—O1 bond. and the intermediate when the proton is bridged between the C1—OH and S=O groups. The distance between the two O atoms in the bridged state is only around 2.56 Å. These are so-called low-barrier hydrogen bonds (LBHB).[37] They are much stronger than the ordinary hydrogen bond, in particular the bridged proton is able to move between the two O atoms freely without any barrier. The formation of LBHB has also been observed during xylose and glucose condensation reactions earlier.[5,6] Based on the reconstructed FES, the barrier associated with protonation of C1—OH is only about 16 kcal/mol and the breakage of C1—O1 bond is about 6 kcal/mol. The overall barrier for protonation of C1—OH and breakage of C1—O1 bond is about 20 kcal/mol. The reaction barrier of 20 kcal/mol is smaller than the corresponding reaction in water, which has a barrier of about 25 kcal/mol. However, the oxocarbenium ion is seen less stable than the initial glucose molecule contrary to the case in aqueous solution indicating proton catalyzed glucose condendation reaction in DMSO is not an energetically favorable process. Our results indicate that solvent could play a critical role in proton catalyzed glucose or other general organic reactions in solution since proton solvation free energy and solvent molecule's proton affinity are typically different in different solvent.

4.2. The mechanism and free energy surface for glucose dehydration reaction in DMSO

The CPMD–MTD simulations for glucose dehydration to the cyclic HMF intermediate were not successful when conducted at the room temperature, or for several other temperatures below 227 °C (500 K). The simulations were successful only after increasing the temperature to 227 °C. This indicates that this dehydration mechanism in DMSO has either a high barrier or is energetically not a favorable process. The schematics of the mechanism for glucose dehydration reaction to form a HMF intermediate via a direct cyclic pathway from CPMD–MTD simulations at 227 °C (500 K) are shown in Figure 5. The reaction is initiated by protonation of the C2—OH on the glucose molecule (***E***). Since the two protons bonded to the O2 atom are indistinguishable, both protons are observed during the sampling process transferring back and forth between the O2 atom

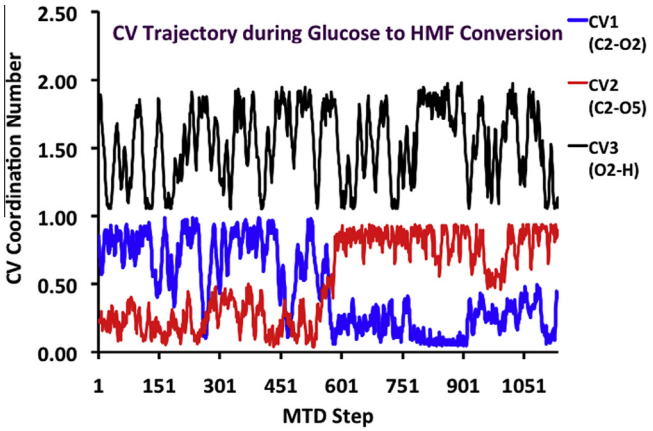

Figure 6. The variation of the CV1 (C2—O2, blue), CV2 (C2—O5, red) and CV3 (O2—H, black) during the CPMD–MTD simulations for glucose dehydration reaction to form HMF in DMSO initiated by protonation of C2—OH.

on glucose and the O atoms of their nearest DMSO molecules. The proton can either be completely transferred or partially transferred via the formation of LBHB to the S=O on a DMSO molecule (***F***). After sufficient sampling, the C2—O2 bond starts to break (***G***). With additional sampling, the C2—O5 bond forms (***H***) and the C1—O5 bond breaks leading to the formation of a five-member ring intermediate (***I***). The subsequently formed $C1^{+}$—OH carbocation is located outside the five-member ring structure. Finally, the O atom on the neighboring DMSO molecule takes away the proton from the O1 leading to the formation of an aldehyde C1H=O intermediate (***J***). The closest two DMSO molecules to the glucose C2—OH act as proton acceptors during the reaction process.

Figure 6 shows the variation of three CVs during the course of over 1100 MTD simulation steps. The proton is initially attached to the C2—OH, but rapidly transfers to the neighboring S=O on the DMSO molecules. During the subsequent sampling process, the proton was seen transferring back and forth between C2—OH and the DMSO molecules. The C2—O2 bond breaks at around 250 MTD steps, but rapidly reforms. The C2—O2 bond was again seen to break at around 450 MTD steps and forms again quickly. The C2—O2 bond is finally broken at 580 MTD steps and remains broken till the end of simulations. On the other hand, the C2—O5 bond only starts to form at around 525 MTD steps and becomes completely bonded at 580 MTD steps. This appears to be different from our CPMD-MTD simulations for glucose dehydration reaction in aqueous solution. The breakage of the C2—O2 bond and the formation of the C2—O5 bond almost occur simultaneously in water. This indicates that the breakage of the C2—O5 bond is not the rate-limiting step during glucose dehydration reaction in aqueous solution. However, in DMSO solvent, breakage of the C2—O5 bond appears to be more difficult and becomes likely the rate-limiting step. Our reconstructed FES confirms that the barrier for C2—O5 breakage is higher than that for C2—O2 breakage, which will be discussed in more detail later. Our continued sampling to about 1100 MTD steps did not lead to the reformation of the glucose reactant as is necessary for obtaining accurate FES due probably to the relative stability of the five member ring intermediate. However, the barrier for the reaction process is generally accurate and reliable as was discussed in our earlier studies.[7,9]

Figure 7 shows the sampling trajectories between CV1 (C2—O2) and CV3 (O2—H) (left panel), and between CV2 (O2—O5) and CV3 (O2—H) (right panel). It can be seen that all three reaction coordinates have extensive sampling indicating the quality of the free energy calculations. Figure 8 exhibits the reconstructed 2D free energy contour plots based on the amount of repulsive potentials added during the 1134 MTD sampling steps. The left panel on Figure 8 shows the 2D free energy contour plot between CV1 and CV3, whereas the right panel on Figure 8 shows the contour plot and FES between CV2 and CV3. It appears that there is only about 5 kcal/mol of barrier associated with the protonation of the C2—OH. The breakage of C2—O2 bond entails another 15 kcal/mol. The overall barrier for protonation of C2—OH and breakage of C2—O2 bond is only about 20 kcal/mol. This barrier is significantly smaller than the 35 kcal/mol barrier observed for protonation of C2—OH and breakage of C2—O2 bond in aqueous solution as shown in our earlier study.[7] This reduction in barrier height is consistent with our understanding of the effects of solvent on sugar reactions. The higher the solvent's affinity for the proton , the more difficult it is for the hydroxyl groups on glucose to compete for the proton and therefore a higher barrier is expected. Since the proton is highly stabilized by the water cluster due to the extensive hydrogen bonding network formed in aqueous solution, the barrier for glucose dehydration reaction is high and largely solvent induced. The glucose dehydration reaction in DMSO is expected to have a different barrier as DMSO's affinity for the proton is different from that of water. Since DMSO cannot form hydrogen bonds with each other, proton transport in DMSO is more localized and likely diffusion limited. As a result, it will be easier for the localized proton to transfer to the neighboring glucose molecule. Thus a lower barrier for protonation of C2—OH in DMSO than in water is expected.

On the hand, the cyclic mechanism for glucose transformation to HMF intermediate involves not only protonation of C2—OH and the breakage of C2—O2 bond, but also the formation of the C2—O5 bond and the breakage of the C1—O5 bond. In our previous study for glucose dehydration to HMF in aqueous solution,[7] the barrier for the formation of C2—O5 bond is only about 20 kcal/mol indicating that protonation of C2—OH and breakage of C2—O2 bond is the rate-limiting step. However, in DMSO solvent, the role appears to be reversed. The formation of C2—O5 bond in DMSO becomes energetically more difficult as shown from the right panel in Figure 8. The barrier for the formation of C2—O5 bond is about 55 kcal/mol in DMSO. This is significantly higher than the reaction in aqueous solution. This is perhaps the reason why our CPMD-MTD simulations for glucose dehydration reaction are successful only when conducted at elevated temperature of 500 K. At a lower temperature, different reaction products were observed.

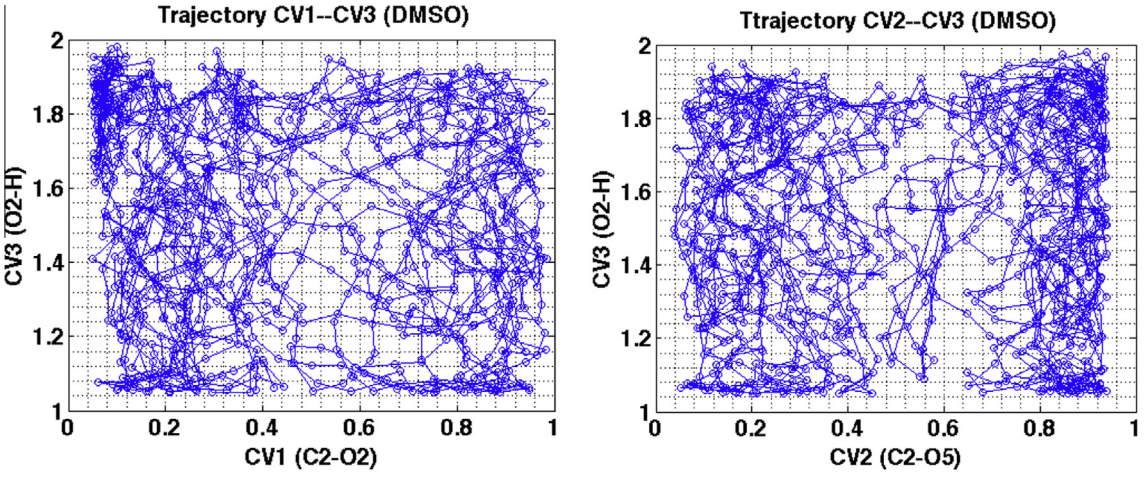

Figure 7. The sampling trajectories between CV1 (C2—O2) and CV3 (O2—H) (left panel), between CV2 (C2—O5) and CV3 (O2—H) (right panel) during CPMD–MTD sampling for glucose dehydration reaction to HMF in DMSO initiated by protonation of C2—OH.

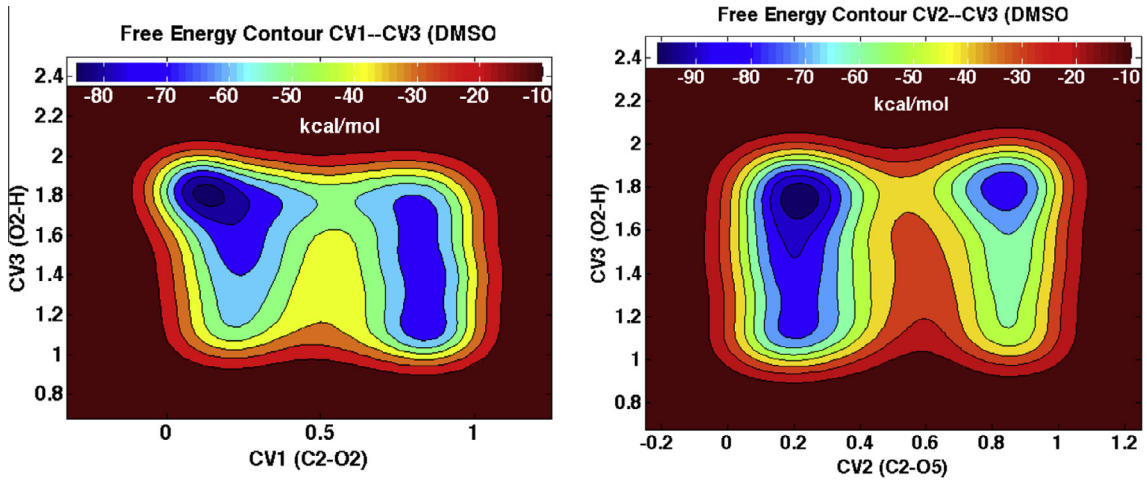

Figure 8. The 2D free energy contour plots between CV1 (C2—O2) and CV3 (O2—H) (left panel), between CV2 (C2—O5) and CV3 (O2—H) (right panel) during the CPMD–MTD sampling for glucose dehydration reaction to HMF in DMSO initiated by protonation of C2—OH.

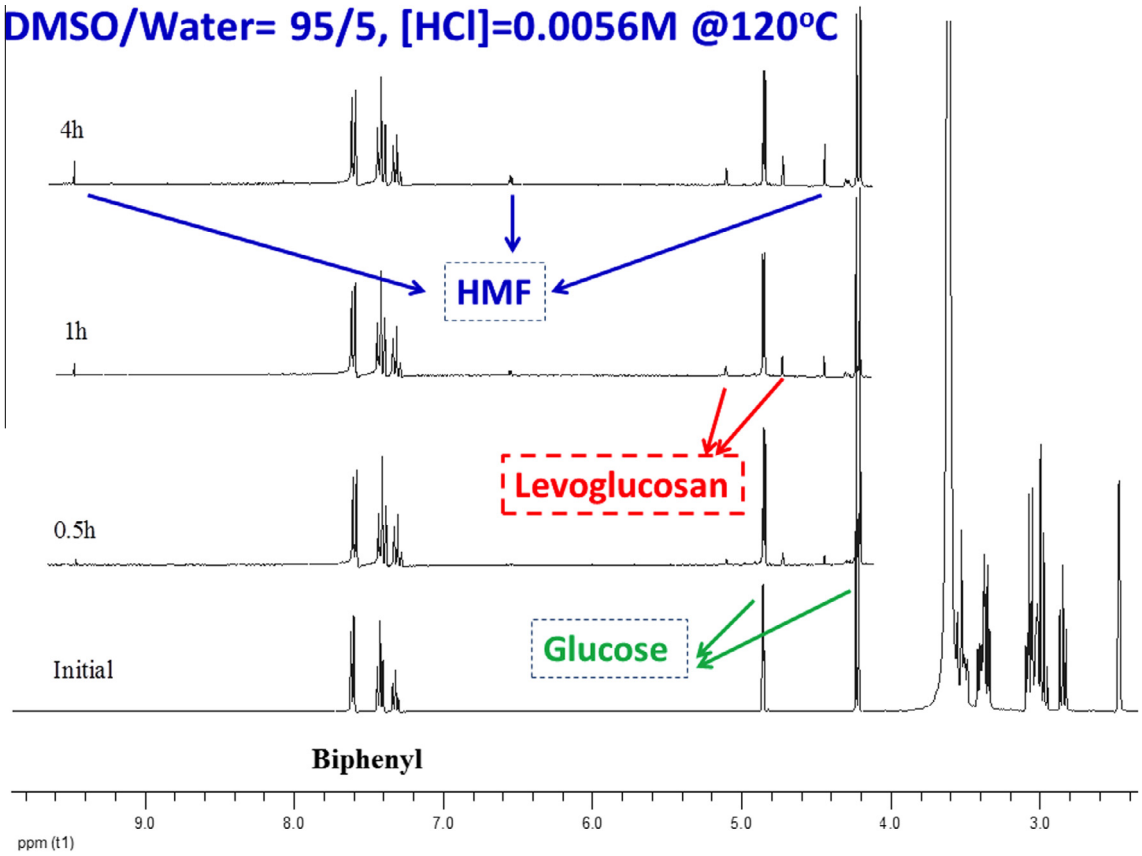

Figure 9. The ^{1}H NMR spectra for glucose conversion in mixed DMSO/Water = 95/5 (v/v) solvent at various times at 120 °C. The peaks for glucose, levoglucosan, and HMF are marked.

4.3. Experimental results on glucose conversion in DMSO and DMSO/Water mixtures

NMR Experiments were conducted to investigate the effects of solvent on glucose dehydration to HMF in pure DMSO and DMSO/Water mixed solvents. Investigated DMSO/Water ratios for the solvent mixtures comprise 100/0, 95/5, 90/10, and 80/20 (v/v). Solvents with higher water contents were not investigated due to the evaporation of water during the experiments. The reactions were conducted at temperatures ranging from 110 °C to 140 °C. Besides HMF, a glucose dehydration product by losing three water molecules, significant amount of 1,6-anhydro-D-β-glucopyranose (levoglucosan), a glucose dehydration product by losing one water molecule was also detected in agreement with earlier studies.[38] Figure 9 shows the NMR spectra for glucose, levoglucosan, and HMF and their respective characteristic peaks for quantitative measurements for glucose in DMSO/Water = 95/5 (v/v) mixed solvent at the beginning and after 0.5, 1, and 4 h of reaction time. It can be

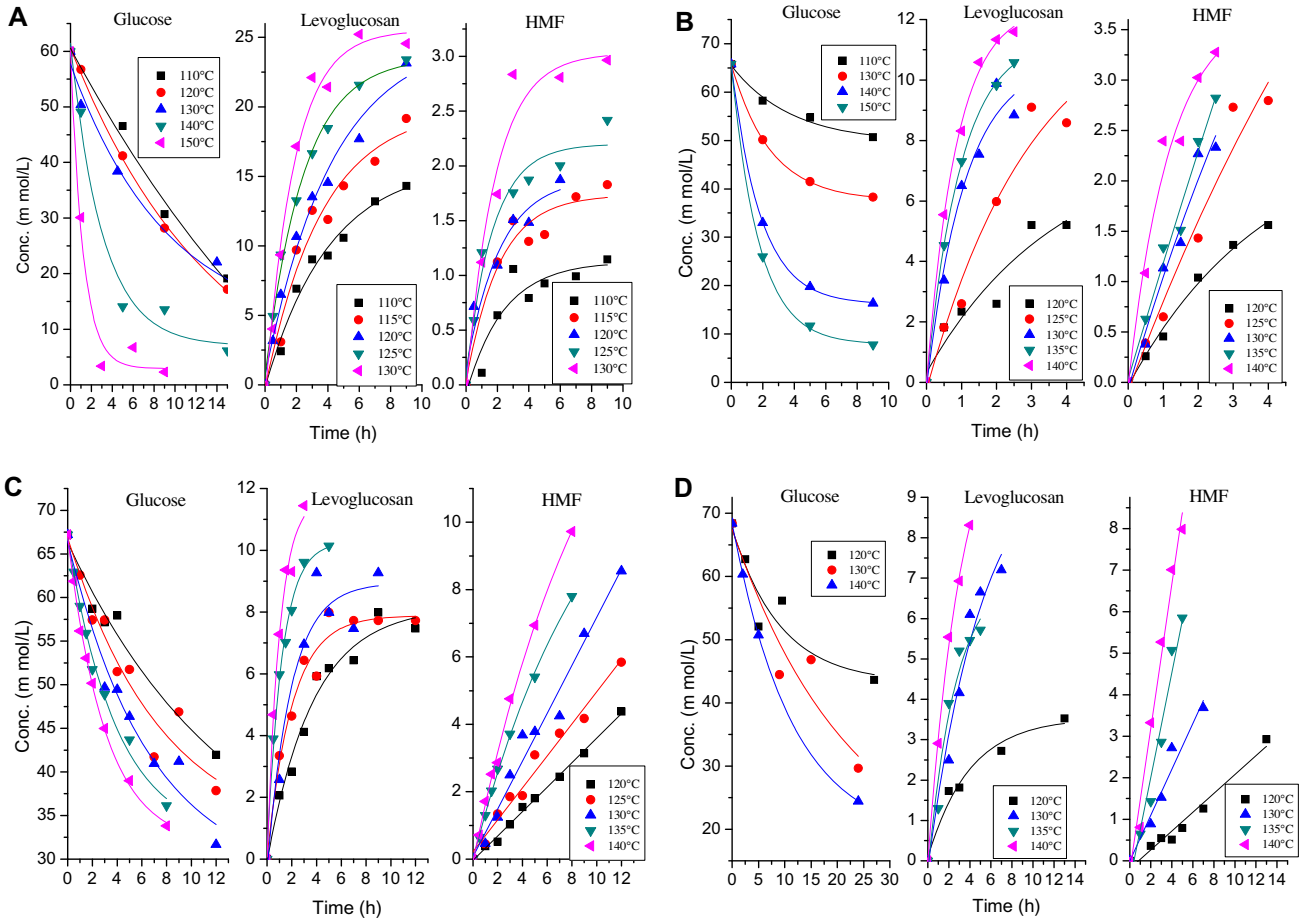

Figure 10. Concentrations of glucose, levoglucosan, and HMF as a function of reaction time are shown for glucose reaction in DMSO (A), and DMSO/Water = 95/5 (B), DMSO/Water = 90/10 (C), and DMSO/Water = 80/20 (D) at various temperatures.

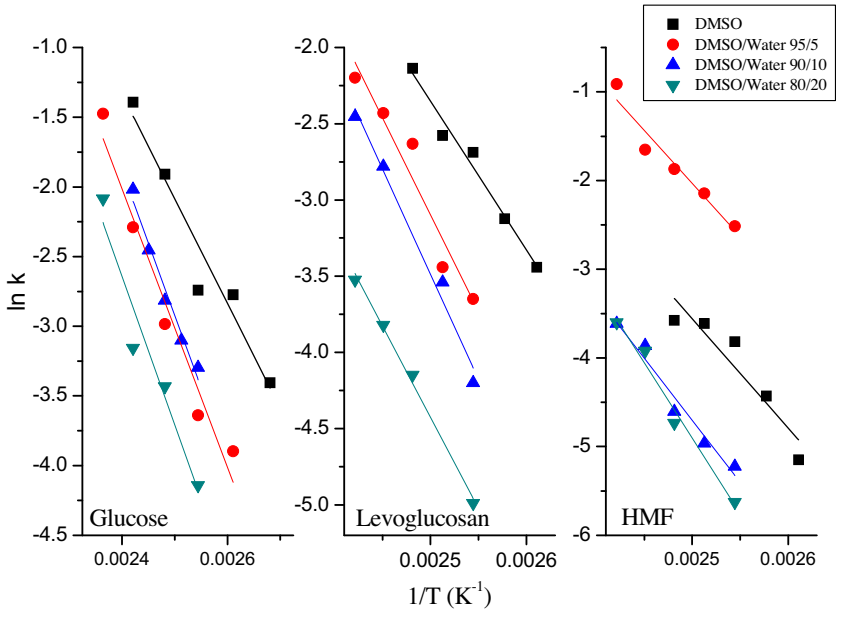

Figure 11. The Arrhenius plots for glucose depletion, levoglucosan, and HMF formation in DMSO and DMSO/Water mixtures.

seen that dehydration product peaks from levoglucosan and HMF keep increasing whereas glucose peaks keep decreasing as the reaction continues. Figure 10 plots the concentrations of glucose, levoglucosan, and HMF as a function of reaction time at various reaction temperatures in DMSO (**A**), DMSO/Water = 95/5 (**B**), DMSO/Water = 90/10 (**C**) and DMSO/Water = 80/20 (**D**) solvents. It can be

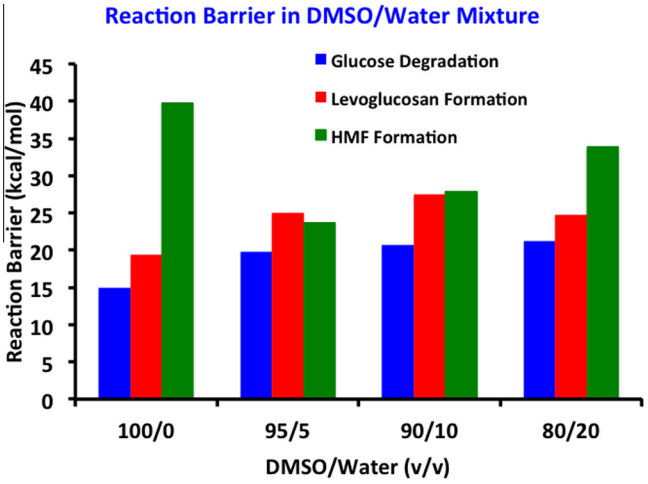

Figure 12. Experimental energy barriers for glucose depletion, levoglucosan, and HMF production in DMSO and DMSO/Water mixtures.

seen that the rate of HMF production increases and the rate of levoglucosan production decreases in solvents as the water content in the solvent mixture increases. The HMF concentration almost reaches a plateau after 4 h of reaction in DMSO solvent whereas it continues to increase linearly in solvents with larger water content with DMSO/Water ratio at 90/10 and 80/20 (v/v). Furthermore, levoglucosan production is much faster in pure DMSO solvent and it slows down significantly when the water content increases. The slow down in HMF production in pure DMSO after 2 h of reaction can be partly caused by the rapid consumption of glucose due to higher rate of levoglucosan production. Nevertheless, it is clear from the data that the reaction rates are strongly solvent dependent.

In order to determine quantitatively the reaction barriers for HMF production in different DMSO/Water solvent mixtures, first-order kinetics are assumed for glucose depletion as well as for HMF and levoglucosan production for the reactions. Figure 11 shows the Arrhenius plots for glucose conversion, HMF, and levoglucosan production at various reaction temperatures in different DMSO/Water mixtures. Based on these Arrenhius plots, the activation barriers for the reactions can be determined. These energy barriers are shown in Figure 12. It can be seen that energy barriers are different in different solvents. For HMF production, the barriers are around 40, 24, 28, and 34 kcal/mol in 100/0, 95/5, 90/10, and 80/20 DMSO/Water ratios respectively. Even though the calculated theoretical barrier is somewhat higher than the experimental value for glucose to HMF conversion in pure DMSO solvent, the overall trend obtained from CPMD–MTD simulations is correct in that HMF production in pure DMSO has a higher barrier than in aqueous solution. On the other hand, levoglucosan appears to have the lowest barrier (19 kcal/mol) in DMSO and the barrier increases with more water content in the mixed solvents (25–27 kcal/mol). This is understandable as water is a product of glucose dehydration. Since glucose conversion to levoglucosan is reversible, the presence of water will slow down or reverse the levoglucosan production.

4.4. The effects of solvent on atomic charges

It is relatively easy to understand why the energy barriers in water and DMSO solvents associated with protonation of C2—OH and the breakage of C2—O2 bond during glucose dehydration reactions are different. However, it is not obvious why the reactivity for the subsequent bonding of C2—O5 is different in the two solvents. Since water is more polar than DMSO, the C2-carbocation is expected to be more stable in water than in DMSO. It seems that bonding between C2—O5 should have a higher energy barrier in water than in DMSO. On the contrary, our calculations show that the formation of C2—O5 bond in aqueous solution has a barrier of about 20 kcal/mol[7] whereas it has significantly a higher barrier of over 50 kcal/mol in DMSO solvent. As a result, the formation of C2—O5 bond becomes the slow and rate-limiting step during glucose dehydration reaction in DMSO. It is known that charge distribution and electrostatic potential play a critical role in chemical reactions in a polar solvent. In order to get a better understanding of the effects of solvent on glucose reactivity, atomic charges based on the electrostatic potential (ESP)[30] were calculated using both Gaussian09 and CPMD codes. The ESP atomic charges of glucose atoms in the gas phase as well as in DMSO or H_2O using implicit CPCM solvation model[32,33,35] were calculated with Gaussian09.

Table 1
Calculated ESP atomic charges for glucose molecule in the gas phase and in H_2O and DMSO solvents

Atom Type	G09 Gas Phase w/o PBC	CPMD Gas Phase w/o PBC	G09 CPCM w/o PBC	CPMD H_2O PBC	CPMD H_2O w/o PBC	CPMD DMSO PBC	CPMD DMSO w/o PBC
C1	0.362	0.486	0.594	−0.504	0.086	1.424	0.347
O1	−0.654	−0.598	−0.723	−0.063	−0.373	−1.05	−0.642
H1(C)	0.033	0.006	0.016	0.502	0.019	−0.227	0.027
C2	0.120	0.123	−0.107	−1.727	0.316	0.317	0.435
O2	−0.693	−0.599	−0.709	0.328	−0.451	−0.811	−0.681
H2(C)	0.113	0.005	0.129	0.734	0.111	−0.247	−0.009
C3	0.220	0.538	0.381	−0.134	0.231	1.308	0.042
O3	−0.699	−0.569	−0.724	−0.38	−0.634	−0.521	−0.465
H3(C)	0.080	−0.028	0.094	0.468	−0.015	−0.438	0.061
C4	0.013	0.096	−0.144	−0.919	0.026	0.559	0.392
O4	−0.694	−0.617	−0.691	−0.167	−0.539	−1.176	−0.738
H4(C)	0.117	0.030	0.134	0.55	0.093	−0.362	0.005
C5	0.138	0.305	0.169	−0.074	0.373	1.544	0.086
O5	−0.471	−0.619	−0.491	−0.05	−0.449	−1.214	−0.478
H5(C)	0.083	0.023	0.076	0.397	0.021	−0.403	0.065
C6	0.263	0.240	0.330	−1.067	0.106	0.682	0.216
O6	−0.684	−0.614	−0.767	−0.266	−0.366	−0.941	−0.647
H6(C,1)	−0.006	0.001	−0.003	0.408	0.013	−0.251	−0.004
H6(C,2)	0.102	0.026	0.084	0.437	0.082	−0.234	0.021

Calculations were also carried out using Gaussian09 with B3LYP functional and 6-311++G** basis set in the gas phase and in DMSO, H_2O solvents with implicit solvation model (CPCM). ESP charges were also calculated for glucose in the gas phase and when the glucose is solvated by explicit H_2O or DMSO molecules using CPMD with BLYP functional both with and without periodic boundary conditions (PBC).

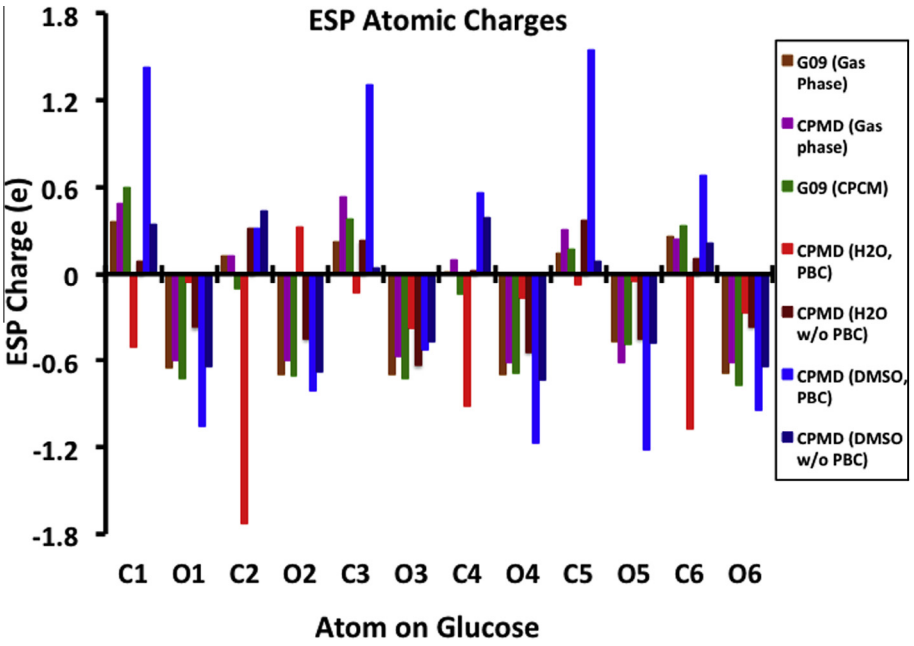

Figure 13. The ESP atomic charges of C and O on glucose in the gas phase, in aqueous solution, and in DMSO solvent at various computation conditions.

Variations in calculated charges are negligible using other implicit solvation methods. The calculated ESP atomic charges for the C, O, and H (C) atoms on glucose are shown in Table 1. To ensure accuracy, the ESP charges for glucose in the gas phase, and when glucose is solvated by the explicit solvent molecules both with and without PBC were also determined using CPMD. The differences in calculated charges using different exchange-correlation functional and plane wave cut-offs on ESP atomic charges are small. However, PBC is found to have a significant influence on the ESP charges. The partial charges for H(O) are not shown in Table 1 as the charges are all between 0.3 and 0.5 for all the —OH groups on glucose from different calculations. The charges on C and O atoms are plotted in Figure 13 in order to illustrate more clearly large charge fluctuations in H_2O and DMSO solvents.

It can be seen that the corresponding atomic charges in the gas phase are very similar to each other calculated by either Gaussian09 or CPMD. Under solution using Gaussian09 with implicit solvation model, the calculated charges on O atoms become slightly more negative. The charges on C2 and C4 also become slightly negative in the solvent whereas charges on C1, C3, and C6 become slightly more positive. The differences in calculated charges using either H_2O or DMSO solvent in the implicit solvent model are negligible. The ESP atomic charges calculated by CPMD with explicit solvent model without PBC are only slightly different from the charges calculated in the gas phase. However, when PBC is applied, the atomic charges of C, O, and H(C) on glucose change dramatically compared to the systems without PBC. The C atoms on glucose become rather negative in H_2O whereas they become highly positive in DMSO. The O atoms on glucose become less negative in H_2O whereas they become more negative in DMSO. In addition, the charges on glucose H(C) become positive in H_2O and negative in DMSO. This indicates that long range electrostatic interaction has a profound impact on the charge distribution of the glucose molecule. The C, O, and H(C) atoms on glucose are highly polarizable and can be strongly affected by their electrostatic environment. However, the H(O) charges are not affected by the specific environment. Earlier studies[39] also indicate that DMSO molecule solvated by H_2O is highly polarizable with an increase of over 81% in dipole moment upon solvation.

As shown in Figure 13, the atomic charges on glucose C and O in H_2O change in the opposite direction to those in DMSO with PBC. This indicates that besides their different proton affinity, DMSO and H_2O solvents affect the charge distribution on glucose rather differently. Because of these differences, the reactivity of glucose in these two solvents is very different. However, it does not explain why the barrier for C2—O5 bond formation is significantly higher in DMSO than in H_2O. Besides the neutral molecule, the charge distribution for the C2-carbocation intermediate is likely to be affected by the solvent as well. Moreover, the stability of the initial glucose structure, the C2-carbocation intermediate and the final cyclic 5-member ring are likely strongly affected by the solvent. All these factors will affect the energetics of the glucose reactions in solution.

5. Conclusion

The mechanisms and the energy barriers for the critical steps during proton catalyzed glucose condensation and dehydration reactions in DMSO were determined. Glucose condensation reaction is initiated by protonation of C1—OH on glucose and subsequent breakage of the C1—O1 bond whereas glucose dehydration reaction is initiated by protonation of C2—OH and the breakage of C2—O2 bond followed by the formation of the C2—O5 bond. The mechanisms are similar to those in the aqueous solutions. However, energy barriers and critical steps are strongly influenced by the solvent molecules. The DMSO molecules are found to participate directly in these reactions as proton acceptors during the reactions. Moreover, the long-range electrostatic interactions appear to influence the reactivity of the glucose molecule substantially through charge redistribution from polarization. Due to strong polarization from the long-range electrostatic interactions, theoretical calculations conducted in the gas phase or using implicit solvent models are generally not accurate for these complex reactions involving carbohydrates. Our experimental results

support the solvent effects on the energy barrier for glucose dehydration to HMF.

Acknowledgements

Funding from NSF CAREER (CBET 1137795) is gratefully acknowledged. Initial structural generation for the calculations by Dr. Hongbo Du is also appreciated. Calculations were carried out on Razor from the High Performance Computing Center (HPC) at the University of Arkansas and Teragrid.

Supplementary data

Supplementary data associated with this article can be found, in the online version, at http://dx.doi.org/10.1016/j.carres.2014.02.010.

References

1. Qian, X. H.; Nimlos, M. R.; Davis, M.; Johnson, D. K.; Himmel, M. E. *Carbohydr. Res.* **2005**, *340*, 2319–2327.
2. Qian, X. H.; Nimlos, M. R.; Johnson, D. K.; Himmel, M. E. *Appl. Biochem. Biotechnol.* **2005**, *121*, 989–997.
3. Qian, X. H.; Johnson, D. K.; Himmel, M. E.; Nimlos, M. R. *Carbohydr. Res.* **2010**, *345*, 1945–1951.
4. Nimlos, M. R.; Qian, X. H.; Davis, M.; Himmel, M. E.; Johnson, D. K. *J. Phys. Chem. A* **2006**, *110*, 11824–11838.
5. Dong, H.; Nimlos, M. R.; Himmel, M. E.; Johnson, D. K.; Qian, X. *J. Phys. Chem. A* **2009**, *113*, 8577–8585.
6. Liu, D. J.; Nimlos, M. R.; Johnson, D. K.; Himmel, M. E.; Qian, X. H. *J. Phys. Chem. A* **2010**, *114*, 12936–12944.
7. Qian, X. H. *J. Phys. Chem. A* **2011**, *115*, 11740–11748.
8. Qian, X. H. *Top. Catal.* **2012**, *55*, 218–226.
9. Qian, X. H.; Wei, X. F. *J. Phys. Chem. B* **2012**, *116*, 10898–10904.
10. Antal, M. J.; Mok, W. S. L.; Richards, G. N. *Carbohydr. Res.* **1990**, *199*, 111–115.
11. Antal, M. J.; Mok, W. S. L.; Richards, G. N. *Carbohydr. Res.* **1990**, *199*, 91–109.
12. Antal, M. J.; Leesomboon, T.; Mok, W. S.; Richards, G. N. *Carbohydr. Res.* **1991**, *217*, 71–85.
13. Pilath, H. M.; Nimlos, M. R.; Mittal, A.; Himmel, M. E.; Johnson, D. K. *J. Agric. Food Chem.* **2010**, *58*, 6131–6140.
14. Qian, X. *J. Phys. Chem. B* **2013**, *117*, 11460–11465.
15. Car, R.; Parrinello, M. *Phys. Rev. Lett.* **1985**, *55*, 2471–2474.
16. CPMD 3.13, copyrighted jointly by IBM Corp and by Max-Planck Institute, Stuttgart.
17. Laio, A.; Parrinello, M. *Proc. Natl. Acad. Sci.* **2002**, *99*, 12562–12566.
18. Frisch, M. J. T.; Trucks, G. W.; Schlegel, H. B.; Scuseria, G. E.; Robb, M. A.; Cheeseman, J. R.; Scalmani, G.; Barone, V.; Mennucci, B.; Petersson, G. A.; Nakatsuji, H.; Caricato, M.; Li, X.; Hratchian, H. P.; Izmaylov, A. F.; Bloino, J.; Zheng, G.; Sonnenberg, J. L.; Hada, M.; Ehara, M.; Toyota, K.; Fukuda, R.; Hasegawa, J.; Ishida, M.; Nakajima, T.; Honda, Y.; Kitao, O.; Nakai, H.; Vreven, T., ; Montgomery, J. A., Jr.; Peralta, J. E.; Ogliaro, F.; Bearpark, M.; Heyd, J. J.; Brothers, E.; Kudin, K. N.; Staroverov, V. N.; Kobayashi, R.; Normand, J.; Raghavachari, K.; Rendell, A.; Burant, J. C.; Iyengar, S. S.; Tomasi, J.; Cossi, M.; Rega, N.; Millam, J. M.; Klene, M.; Knox, J. E.; Cross, J. B.; Bakken, V.; Adamo, C.; Jaramillo, J.; Gomperts, R.; Stratmann, R. E.; Yazyev, O.; Austin, A. J.; Cammi, R.; Pomelli, C.; Ochterski, J. W.; Martin, R. L.; Morokuma, K.; Zakrzewski, V. G.; Voth, G. A.; Salvador, P.; Dannenberg, J. J.; Dapprich, S.; Daniels, A. D.; Farkas, Ö.; Foresman, J. B.; Ortiz, J. V.; Cioslowski, J.; Fox, D. J. *Gaussian 09 Revision A.1*; Gaussian: Wallingford CT, 2009.
19. Iannuzzi, M.; Laio, A.; Parrinello, M. *Phys. Rev. Lett.* **2003**, *90*, 238302.
20. Dong, H.; Qian, X. Ab Initio Molecular Dynamics Investigation of Xylan Hydrolysis In *Computational Modeling in Lignocellulosic Biofuel Production*; Nimlos, M. R., Crowley, M. F., Eds.; ACS Symposium Series, 2011; pp 1–15.
21. Ensing, B.; De Vivo, M.; Liu, Z.; Moore, P.; Klein, M. L. *Acc. Chem. Res.* **2006**, *39*, 73–81.
22. Becke, A. D. *Phys. Rev. A* **1988**, *38*, 3098–3100.
23. Lee, C. T.; Yang, W. T.; Parr, R. G. *Phys. Rev. B* **1988**, *37*, 785–789.
24. Goedecker, S.; Teter, M.; Hutter, J. *Phys. Rev. B* **1996**, *54*, 1703–1710.
25. Qian, X. H. *Mol. Simul.* **2008**, *34*, 183–191.
26. Qian, X. H.; Ding, S. Y.; Nimlos, M. R.; Johnson, D. K.; Himmel, M. E. *Macromolecules* **2005**, *38*, 10580–10589.
27. Nose, S. *J. Chem. Phys.* **1984**, *81*, 511–519.
28. Hoover, W. G. *Phys. Rev. A* **1985**, *31*, 1695.
29. Ewald, P. *Ann. Phys.* **1921**, *64*, 253–287.
30. Singh, U. C.; Kollman, P. A. *J. Comput. Chem.* **1984**, *5*, 129–145.
31. Hirshfeld, F. L. *Theor. Chim. Acta* **1977**, *44*, 129–138.
32. Liptak, M. D.; Shields, G. C. *Int. J. Quantum Chem.* **2001**, *85*, 727–741.
33. Toth, A. M.; Liptak, M. D.; Phillips, D. L.; Shields, G. C. *J. Chem. Phys.* **2001**, *114*, 4595–4606.
34. Tissandier, M. D.; Cowen, K. A.; Feng, W. Y.; Gundlach, E.; Cohen, M. H.; Earhart, A. D.; Coe, J. V.; Tuttle, T. R. *J. Phys. Chem. A* **1998**, *102*, 7787–7794.
35. Dong, H.; Du, H.; Qian, X. *J. Phys. Chem. A* **2008**, *112*, 12687–12694.
36. Kelly, C. P.; Cramer, C. J.; Truhlar, D. G. *J. Phys. Chem. B* **2006**, *111*, 408–422.
37. Cleland, W. W.; Kreevoy, M. M. *Science* **1994**, *264*, 1887–1890.
38. Ohara, M.; Takagaki, A.; Nishimura, S.; Ebitani, K. *Appl. Catal. A: Gen.* **2010**, *383*, 149–155.
39. Kirchner, B.; Hutter, J. *J. Chem. Phys.* **2004**, *121*, 5133–5142.